Petroleum Science 20 (2023) 2386–2398

Contents lists available at ScienceDirect

Petroleum Science

journal homepage: www.keaipublishing.com/en/journals/petroleum-science

Original Paper

In-situ pressure-preserved coring for deep exploration: Insight into the rotation behavior of the valve cover of a pressure controller

Da Guo [a, b, c], He-Ping Xie [b, c], Ling Chen [a, b, *], Zhong-Ya Zhou [d], He-Ping Lu [d], Lin Dai [d], Ding-Ming Wang [b], Tian-Yu Wang [b], Ju Li [a], Zhi-Qiang He [b], Yun-Qi Hu [a, b, c], Ming-Zhong Gao [b, c]

[a] School of Mechanical Engineering, Sichuan University, Chengdu, Sichuan, 610065, China
[b] MOE Key Laboratory of Deep Underground Science and Engineering, College of Water Resource and Hydropower, Sichuan University, Chengdu, Sichuan, 610065, China
[c] Guangdong Provincial Key Laboratory of Deep Earth Sciences and Geothermal Energy Exploitation and Utilization, Institute of Deep Earth Sciences and Green Energy, College of Civil and Transportation Engineering, Shenzhen University, Shenzhen, Guangdong, 518060, China
[d] Petroleum Engineering Technology Research Institute of Sinopec Jianghan Oilfield Company, Wuhan, Hubei, 430035, China

ARTICLE INFO

Article history:
Received 12 August 2022
Received in revised form
30 November 2022
Accepted 19 February 2023
Available online 23 February 2023

Edited by Jia-Jia Fei

Keywords:
In-situ coring
Pressure coring
Pressure controller
Rotation behavior
Drilling fluid

ABSTRACT

In-situ pressure-preserved coring (IPP-Coring) is considered to be the most reliable and efficient method for the identification of the scale of oil and gas resources. During IPP-Coring, because the rotation behavior of the pressure controller valve cover in different medium environments is unclear, interference between the valve cover and inner pipe may occur and negatively affect the IPP-Coring success rate. To address this issue, we conducted a series of indoor experiments employing a high-speed camera to gain greater insights into the valve cover rotation behavior in different medium environments, e.g., air, water, and simulated drilling fluids. The results indicated that the variation in the valve cover rotation angle in the air and fluid environments can be described by a one-phase exponential decay function with a constant time parameter and by biphasic dose response function, respectively. The rotation behavior in the fluid environments exhibited distinct elastic and gravitational acceleration zones. In the fluid environments, the density clearly impacted the valve cover closing time and rotation behavior, whereas the effect of viscosity was very slight. This can be attributed to the negligible influence of the fluid viscosity on the drag coefficient found in this study; meanwhile, the density can increase the buoyancy and the time period during which the valve cover experienced a high drag coefficient. Considering these results, control schemes for the valve cover rotation behavior during IPP-Coring were proposed for different layers and geological conditions in which the different drilling fluids should be used, e.g., the use of a high-density valve cover in high-pore pressure layers.

1. Introduction

Shallow earth resources are increasingly exhausted, and resource development is gradually moving toward the deep earth, which has become a scientifically and technologically important topic in global energy development (He et al., 2022; Xie et al., 2015, 2020, 2021). With the ongoing resources transitioning to the deep earth, the exploration and evaluation of deep resources have become the main approach for realizing the strategic replacement of oil and gas resources (Aydin, 2015; Gautam et al., 2022; Wang et al., 2017). Notably, during exploration in the mining and petroleum industries, the coring process is usually considered to be the most reliable and important method to identify the scale of oil, gas, and mineral resources (Mahzari et al., 2021). By analyzing the properties of the obtained core samples, such as the porosity, permeability, and saturation, reservoir properties can be further identified (Ashena, 2017; Ashena and Thonhauser, 2018). However, for conventional coring with no pressure preservation capacity during tripping, the core fluid can be expelled due to the pressure

* Corresponding author. School of Mechanical Engineering, Sichuan University, Chengdu, Sichuan, 610065, China.
E-mail address: chenlingscu@scu.edu.cn (L. Chen).

https://doi.org/10.1016/j.petsci.2023.02.020

difference, and therefore, the real rock composition and occurrence state may be destroyed (Ali et al., 2014; Bjorum, 2013; Davis et al., 2013; Huang et al., 2021; Hyland, 1983; Li et al., 2022b; Mukherjee et al., 2018). To address this problem, *in-situ* pressure-preserved coring (IPP-Coring) has been introduced in deep exploration over the last few decades (Davis et al., 2013; Hyland, 1983; Kawasaki et al., 2006; Kvenvolden et al., 1983; Mukherjee et al., 2018; Al Saman Al Neaimi et al., 2014; Sun et al., 2015b).

In the IPP-Coring process, a core under *in-situ* pressure can be retrieved using a completely sealed device. In this device, the most essential and problematic component is the automatic sealing assembly at the bottom of the coring device. This assembly must not only provide a sufficient inner diameter to allow the passage of the core during coring but also provide a bottom hole auto closure function after core entry in the device to achieve *in-situ* pressure preservation. Ball and flapper valves are two commonly used automatic sealing assemblies in the existing IPP-Coring devices (Hu et al., 2022). The pressure core barrel (PCB), which was used in the Deep Sea Drilling Project (DSDP), and the pressure core sampler (PCS) adopted in the international Ocean Drilling Program (ODP) are two typical devices employing a ball valve as the automatic sealing assembly (Dickens et al., 1997, 2003; Kvenvolden et al., 1983). However, due to the easy occurrence of a sticking problem of the ball valve in the auto closure procedure, the success rate of these two devices is low (Li et al., 2022a). By contrast, the flapper valve can provide better vibration resistance and does not easily become stuck in the auto closure procedure. Therefore, the flapper valve is more suitable for use in deep IPP-Coring to obtain a large-diameter core under *in-situ* pressure (Hu et al., 2022). For this reason, this valve type has been installed in many IPP-Coring devices, such as the Fugro pressure corer (FPC), hydrate auto-clave coring equipment (HY-ACE) rotary corer (HRC) (Burger et al., 2003), and pressure and temperature preservation system (PTPS) (Zhu et al., 2013). Representative IPP-Coring devices and their corresponding automatic sealing assembly and pressure-maintaining capacity are summarized in Table 1.

As indicated in Table 1, the pressure preservation capacity of the existing flapper valve is relatively poor ($\leq$ 30 MPa), and thus, it cannot meet the pressure requirements of deep coring. Based on the basic structure of the flapper valve, we designed a new automatic sealing assembly using the Steinmetz solid structure, namely, the pressure controller, and showed that its pressure-maintaining capacity reached 100.9 MPa (He et al., 2019; Li et al., 2021). The operation process and a photograph of the pressure controller are shown in Fig. 1. At the drilling stage, the valve cover is opened. When the core has completely entered the core pipe, the core and inner pipes are driven upward under the action of a salvage device or the hydraulic pressure of the drilling fluids (Hu et al., 2022; Zhu et al., 2011). At this time, the spring is compressed, and the limit of the valve cover is released. Subsequently, the valve cover is triggered by an elastic piece on the back side, and is closed under gravity. At the same time, the spring is released, then the inner pipe is pressed the valve cover to realize initial sealing.

The above indicates that successful pressure preservation requires the valve cover to be closed before the inner pipe rebound process. After the valve cover is closed, the inner pipe should quickly press the valve cover to ensure the realization of the initial sealing. Notably, as shown in Fig. 1b, if the rotation velocity of the valve cover is lower than the rebound speed of the inner pipe, the valve cover may collide and interfere with the inner pipe, leading to loss of the rotational stability of the valve cover, which may further lead to failure of accurate contact realization between the sealing areas of the valve cover and valve seat. This may result in failure of the IPP-Coring process. By contrast, if the rotation velocity of the valve cover is higher than the rebound speed of the inner pipe, the initial sealing pressure cannot be provided in time after valve cover closure, leading to the leakage of the *in-situ* pressure. Thus, the rotation behavior of the valve cover is critical for the success rate of the IPP-Coring process.

In the IPP-Coring process, the rotation behavior of the valve cover is mainly affected by the medium environment (air, water, and drilling fluid). However, although much systematic research on IPP-Coring has been performed, most studies have only focused on the pressure preservation capacity (Abid et al., 2015; He et al., 2019; Li et al., 2021, 2022a; Sahu et al., 2020). There has been a lack of studies regarding the rotation behavior of the valve cover. Because the rotation behavior of the valve cover in different medium environments is unclear, the problem of interference often occurs during IPP-Coring, reducing the success rate of the IPP-Coring process. To improve the IPP-Coring success rate, it is necessary to better understand the valve cover rotation behavior in different environments.

In this study, according to the actual service environment of the pressure controller, the rotation behavior of the valve cover of the pressure controller in air, water, and simulated drilling fluids was clarified via a high-speed camera. Through a thorough analysis of the rotation process and variation in the drag coefficient of the valve cover in the different environments, the mechanisms of the rotation behavior of the valve cover in the different environments was revealed. Based on the results, control schemes for the rotation behavior of the valve cover during IPP-Coring in different layers and geological conditions were proposed.

2. Experiments and methods

2.1. Design of the experimental medium environments

In this study, the rotation behavior of the valve cover of the pressure controller was investigated in air, water, and simulated drilling fluid environments according to the actual service

Table 1
Summary of the different IPP-Coring devices.

IPP-Coring devices	Institutions	Automatic sealing assembly	Pressure
PCB (Kvenvolden et al., 1983)	DSDP	Ball valve	$\leq$ 35 MPa
PCS (Dickens et al., 1997, 2003)	ODP	Ball valve	$\leq$ 69 MPa
FPC (Burger et al., 2003)	EU-sponsored HYACINTH program	Flapper valve	$\leq$ 25 MPa
HRC (Burger et al., 2003)	EU-sponsored HYACINTH program	Flapper valve	$\leq$ 25 MPa
PTCS (Kawasaki et al., 2006)	Japan Oil, Gas and Metals National Corporation (JOGMEC)	Ball valve	$\leq$ 30 MPa
Pressure tight piston corer (PTPC) (Qin et al., 2005)	Zhejiang University	Flapper valve	$\leq$ 30 MPa
PTPS (Zhu et al., 2013)	China University of Petroleum, Beijing	Flapper valve	$\leq$ 30 MPa
GWY194-70BB (Yang et al., 2014)	Great Wall Drilling Company of the China National Petroleum Corporation (CNPC)	Ball valve	$\leq$ 20 MPa
GW-CP194-80A (Yang et al., 2020)	Great Wall Drilling Company of the CNPC	Ball valve	$\leq$ 60 MPa

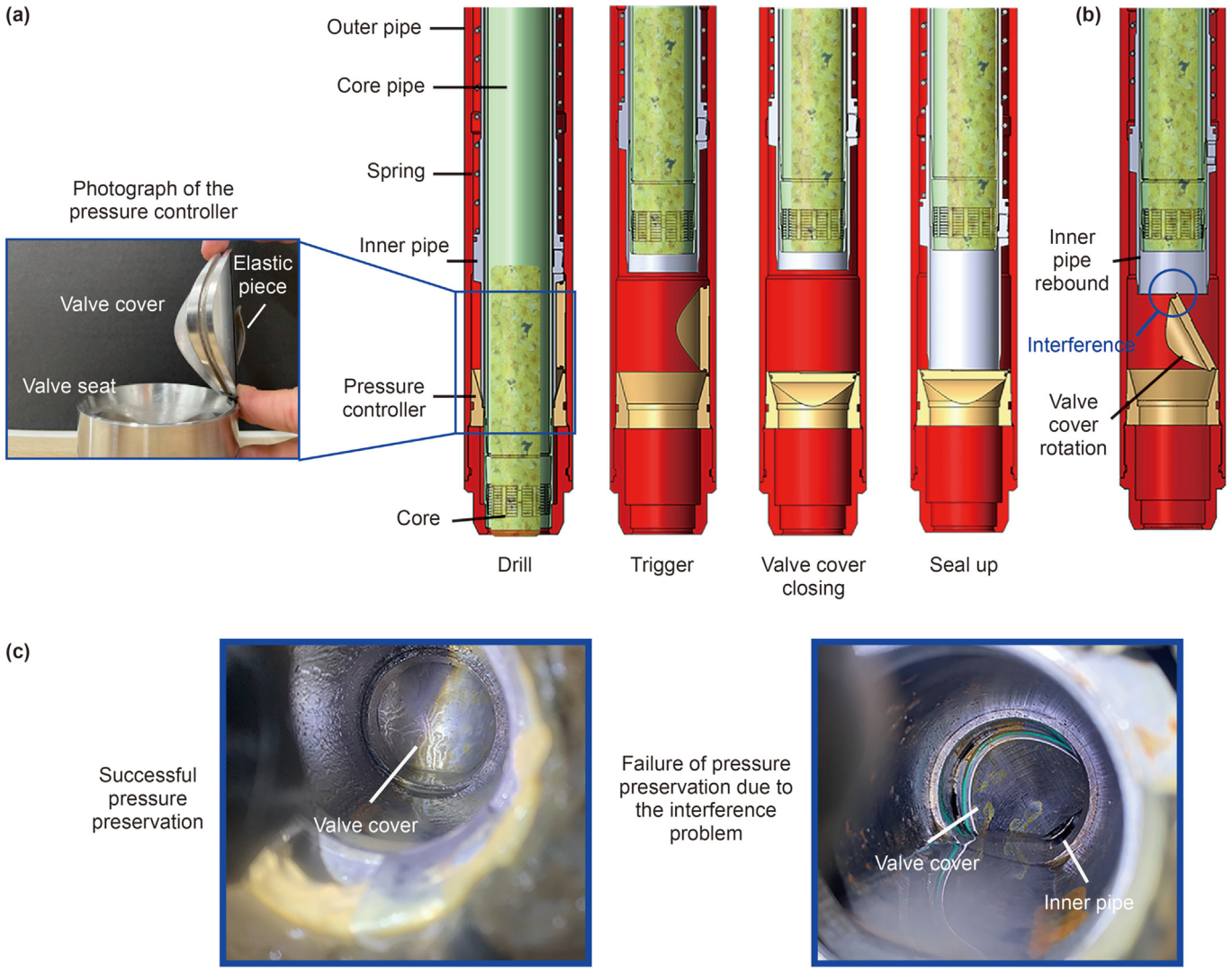

Fig. 1. (**a**) Operation process and photograph of the pressure controller, (**b**, **c**) schematic and field photograph of the interference problem during IPP-Coring.

environment of the pressure controller. In the drilling industry, the commonly used drilling fluids include dispersed drilling fluids, brine drilling fluids, polymer-based drilling fluids, and synthetic-based drilling fluids. Among these drilling fluids, the brine drilling fluid system is a Newtonian fluid, while the other drilling fluids are non-Newtonian fluids (Zhang, 2019; Mahmoud et al., 2020). In this study, to ensure that the obtained experimental results can closely reflect field conditions and that the rotation behavior of the valve cover can be accurately captured, aqueous potassium formate (KCOOH) and xanthan gum (XC) solutions were selected to simulate Newtonian and non-Newtonian drilling fluids, respectively. The experimental groups are summarized in Table 2, and the viscosity and density of the solutions listed in Table 2 were measured with a six-speed rotational viscometer (KC-6ST, China) and balance hydrometer (MC, China), respectively.

Table 2
Experimental groups.

No.	Medium environment	Mass concentration, %
1	Air	~
2	Water	~
3	KCOOH aqueous solution	56
4	KCOOH aqueous solution	76
5	XC aqueous solution	0.05
6	XC aqueous solution	0.15

2.2. Experiments and setup

Fig. 2 shows a schematic diagram and a photograph of the experimental setup. A high-speed camera (NAC Memrecam HX-7s, Japan) was used to capture and record the rotation trajectories of the valve cover of the pressure controller. The recording rate of the camera in this study was set to 0.002 s, which is fast enough to gain insights into the rotation behavior of the valve cover of the pressure controller. The density and the mass of the valve cover are 7.93 g/cm^3 and 244.26 g, respectively, and the material of the valve cover is 304 steel. As shown in Fig. 2b, behind and at 45° to the side of the camera, two lamps were positioned for illumination. Prior to the experiments, the pressure controller with an opened valve cover was placed in the outer pipe (transparent acrylic pipe), with an inner diameter of 80 mm, and the inner pipe was used to restrain the motion range of the valve cover. Then, in the experimental groups with the different fluid environments, solutions were poured into the pipe and remained static. Thereafter, the inner tube

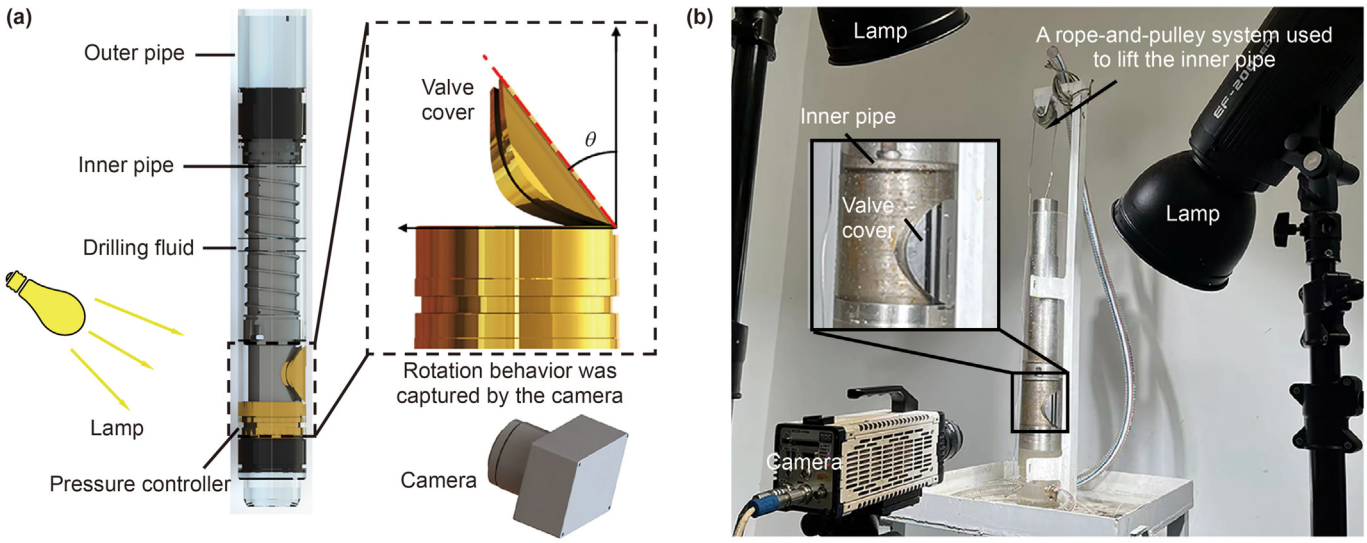

Fig. 2. (**a**) Schematic diagram of the experiments; (**b**) photograph of the experimental setup.

was lifted through a rope-and-pulley system, and the restraint of the valve cover was released. Furthermore, the valve cover was rotated, and its trajectories were captured and recorded with the camera. The experiments were conducted under atmospheric pressure at a temperature of 26 ± 1 °C. All experiments were repeated three times to obtain reliable data. The average total closing time of the three repeated experiments was taken as the closing time of the valve cover in different environments. For different environments, the experiment in which the total close time of the valve cover was the closest to the average time was selected to analyze the rotation behavior of the valve cover. As shown in the inset figure of Fig. 2b, to accurately identify the angle of the valve cover, two black parallel lines were marked on the surface of the valve cover. The slope of the two black parallel lines was obtained at each instance via an image processing algorithm. Then, the transient angle of the valve cover, as shown in Fig. 2a, and the total closing time of the pressure controller were determined. For the transient angle data obtained through image processing, a fitted curve was used as the final angle versus time curve. Furthermore, the instantaneous angular velocity and angular acceleration were determined by calculating the first and second derivatives of the fitted curve, respectively.

3. Results

3.1. Physical parameters of the simulated drilling fluids

The physical parameters of the simulated drilling fluids are shown in Fig. 3. As shown in Fig. 3a, for the KCOOH solutions with different concentrations, the density increased substantially with increasing concentration. The density of the 76% KCOOH solution was 1.214 and 1.565 times larger than those of the 56% KCOOH solution and water, respectively. By contrast, for the XC solutions with different concentrations, the density remained almost constant, approaching that of water. However, for both the KCOOH and XC solutions, as shown in Fig. 3b, the apparent viscosity markedly increased with increasing concentrations. The apparent viscosity of the 76% KCOOH solution reached 11.85 mPa s, which was the highest among the four solutions and 59.2 times higher than the viscosity of water. However, when the concentration of the KCOOH solution was reduced to 56%, the apparent viscosity (AV) declined sharply to 2.45 mPa s. This value was 0.9 and 5.9 mPa s lower than those of the 0.05% and 0.15% XC solutions, respectively, and was 12.25 times higher than that of water. Fig. 3c and d respectively show rheological curves for the KCOOH and XC solutions with different concentrations. The curves in Fig. 3c indicate that the rheological characteristics of the KCOOH solutions in this study fit the characteristics of a Newtonian fluid. Based on Fig. 3d, the rheological characteristics of the XC solutions match those of non-Newtonian fluids and can be described by a power-law fluid model.

3.2. Closing time of the valve cover in the different environments

The closing time of the valve cover affects the success rate of the IPP-Coring operation. If the closing time of the valve cover is too long, the valve cover may interfere with the inner tube in the closing process, which may cause the moving valve cover to lose its balance. As a result, the sealing surfaces of the valve cover and valve seat may not achieve close contact, thus failing to preserve the *in-situ* pressure. Therefore, it is necessary to analyze the total closing time of the valve cover in the different environments. Fig. 4 shows the closing time of the valve cover of the pressure controller in the different experimental environments. The valve cover in the air environment exhibited the shortest closing time of 0.164 s, followed by a closing time of 0.408 s in the water environment. The valve cover in the 76% KCOOH solution environment that exhibits the highest density attained the longest closing time of 0.626 s that is 3.82 and 1.53 times higher than those in the air and water environments, respectively. In addition, for the KCOOH solutions, with decreasing concentration from 76% to 56%, the closing time decreased to 0.533 s; however, it remained 1.31 times longer than that in the water environment. It should be noted that the density of the XC solutions approached that of water, but their apparent viscosity was higher than that of water and the 56% KCOOH solution. However, the closing time of the valve cover in both the 0.05% and 0.15% XC solution environments was close to that in the water environment, indicating that the viscosity had a negligible influence on the closing time of the valve cover. Overall, it was concluded that the solution density clearly affected the closing time of the valve cover, whereas the effect of the viscosity was very weak.

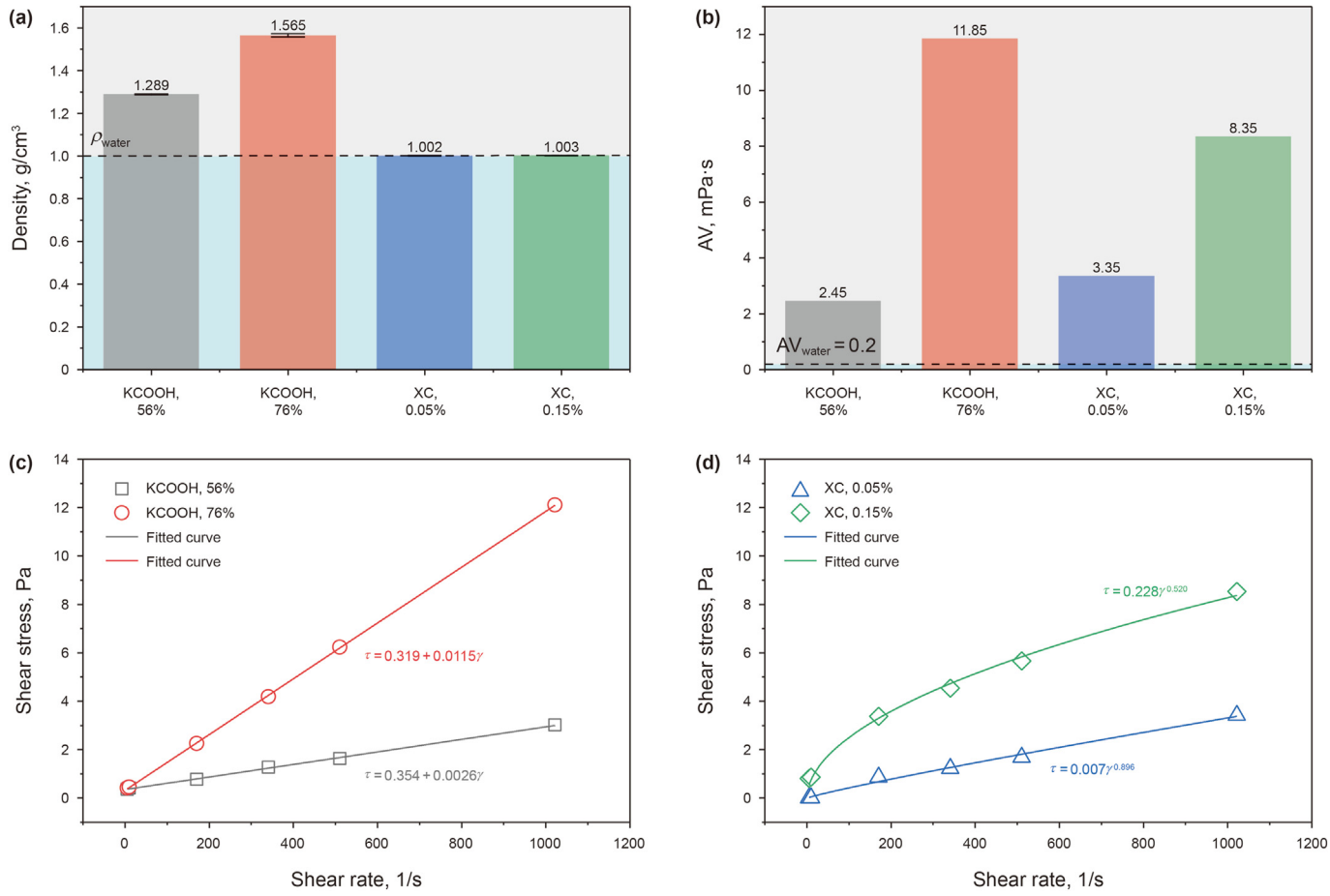

Fig. 3. Physical parameters of the simulated drilling fluids: (**a**) density, (**b**) apparent viscosity (AV), and (**c**, **d**) rheological curves for the KCOOH and XC solutions indicating that these solutions are typical Newtonian and non-Newtonian fluids, respectively.

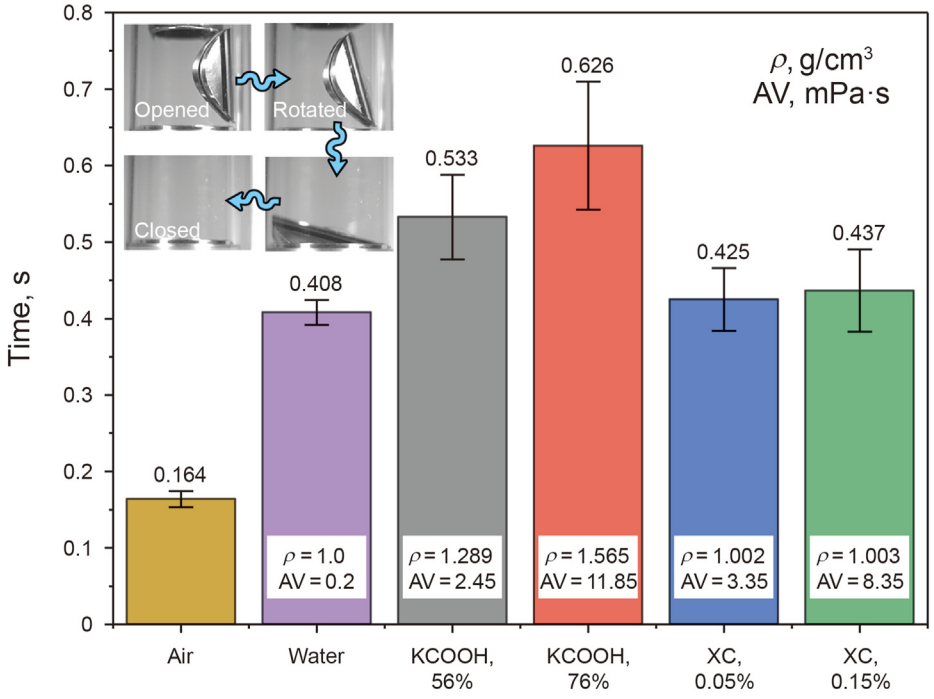

Fig. 4. Closing time of the valve cover of the pressure controller in the different medium environments.

3.3. Rotation behavior of the valve cover

In the IPP-Coring process, movement interference between the inner pipe and valve cover of the pressure controller can only occur during rotation of the valve cover. To prevent the occurrence of interference and increase the IPP-Coring success rate, it is necessary to elucidate the rotation behavior of the valve cover and gain insight into the variation in the rotation angle of the valve cover over time in the different environments.

3.3.1. Rotation behavior of the valve cover in the air environment

When the coring operation is performed in soil and soft rock layers, to prevent contamination of the obtained core samples with the drilling fluid, a dry drilling process is often adopted. In this case, the valve cover of the pressure controller is rotated in an air environment. Fig. 5 shows the rotation behavior of the valve cover of the pressure controller in the air environment. As shown in Fig. 5a, the characteristics of the variation in the rotation angle of the valve cover of the pressure controller in the air environment can be described via a one-phase exponential decay function with a constant time parameter (ExpDec1 function). Furthermore, the first and second derivatives of this function can be calculated to obtain the instantaneous angular velocity and angular acceleration, respectively, of the valve cover in the air environment. As shown in Fig. 5b, when the inner pipe was lifted, the elastic piece on the back side of the valve cover rapidly provided it with an initial angular velocity of 206°/s and an angular acceleration of 2050°/s^2, after which the valve cover began to rotate. In the air environment, both the angular velocity and angular acceleration of the valve cover increased exponentially over time. At approximately 0.16 s, the angular velocity of the valve cover reached the maximum value of 1010°/s, and the valve cover was closed at the same time. Generally, the variation in the rotation angle of the valve cover in the air environment can be described with the ExpDec1 function, and the angular velocity and angular acceleration of the valve cover exponentially increased over time.

3.3.2. Rotation behavior of the valve cover in the fluid environment

In the practice of IPP-Coring, the dry drilling process is only used in a few unique cases. In most cases, drilling fluids should be adopted to cool the bit, clean the borehole, and maintain the stability of the borehole wall. In the IPP-Coring process for deep coalbed methane exploitation, to reduce the reservoir damage due to the drilling fluid and further improve the quality of the obtained *in-situ* coal samples, water is often used as the drilling fluid (Gao et al., 2021; You et al., 2022). In this case, the valve cover of the pressure controller is rotated in a water environment. Fig. 6 shows the rotation behavior of the valve cover of the pressure controller in the water environment. Interestingly, as shown in Fig. 6a, the variation in the rotation angle in the water environment can be described with a biphasic dose response function (BiDoseResp function). Furthermore, to better understand the rotation behavior, the first and second derivatives of this function were calculated to obtain the angular velocity and angular acceleration, respectively. As shown in Fig. 6b, the black curve shows the variation in the angular velocity, and the red curve shows the variation in the angular acceleration. In the water environment, two clear acceleration zones occurred in the rotation process of the valve cover that were produced by the elastic force of the elastic piece on the back side of the valve cover and the gravity of the valve cover itself. In the rotation process of the valve cover, when the rotation angle was smaller than 10°, elastic action occurred, and this zone was defined as the elastic acceleration zone. In the elastic acceleration zone, when the inner pipe was lifted, the elastic piece rapidly provided the valve cover with an initial velocity of 180°/s. This value is 26°/s lower than that in the air environment due to the higher initial drag force and adhesion of the back side of the valve cover to the outer pipe in the water environment. Then, the valve cover was mainly driven by the elastic force to approximately 10° within 0.04 s. Thereafter, from 0.04 to 0.12 s, the dominant driving force of the valve cover changed from the elastic force to gravity, and the valve cover was rotated from 10° to 24°. Later, in the 0.12–0.24 s time period, the valve cover entered the gravitational acceleration zone and was completely accelerated by gravity. After 0.24 s, the angular velocity started to decrease. In addition, the angular acceleration declined below zero and continued to decrease from 0.24 to 0.32 s. Overall, the variation in the rotation angle of the valve cover in the water environment can be described with the BiDoseResp function, and the rotation behavior revealed distinct elastic and gravitational acceleration zones.

Due to the poor performance of clean water in borehole cleaning and borehole wall stability maintenance, other drilling fluid systems, such as brine and polymer-based drilling fluids, are often applied in different formations in IPP-Coring for deep oil and gas exploration (Sun et al., 2015a). To ensure that the obtained experimental results closely represent field conditions and that the

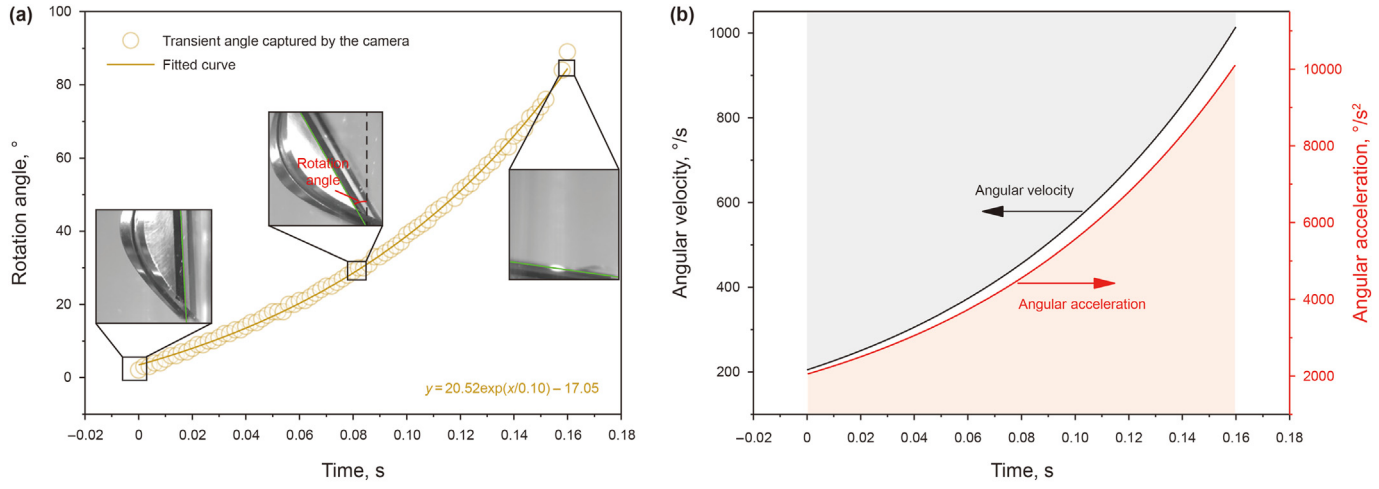

Fig. 5. Rotation behavior of the valve cover of the pressure controller in the air environment: (**a**) variation in the rotation angle; (**b**) variation in the angular velocity (black curve) and variation in the angular acceleration (red curve).

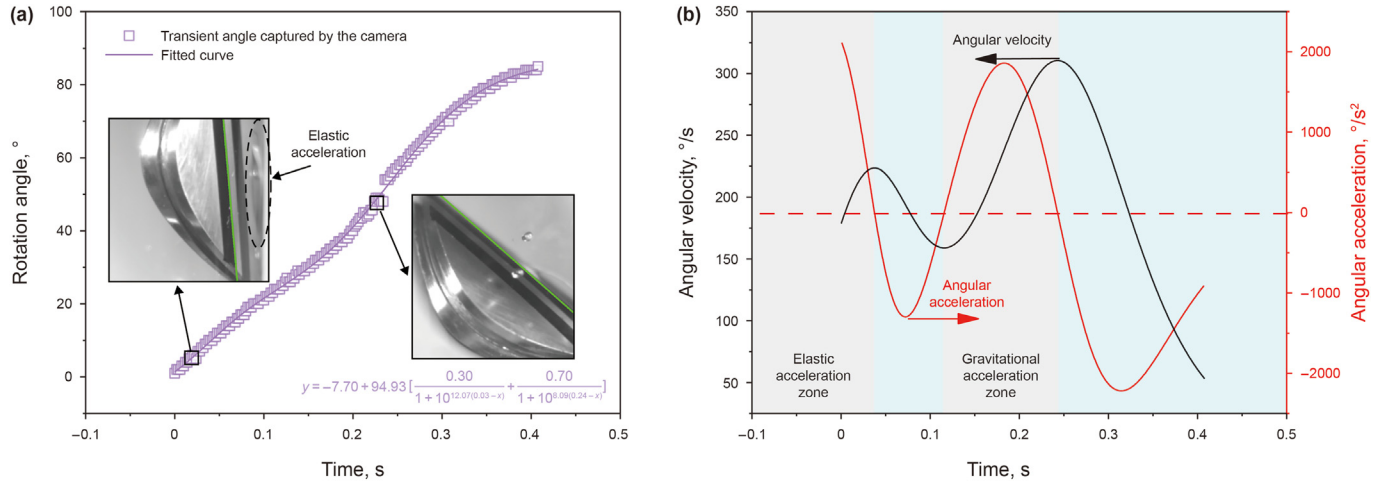

Fig. 6. Rotation behavior of the valve cover of the pressure controller in the water environment (ρ = 1.0 g/cm^3; AV = 0.2 mPa s): (**a**) variation in the rotation angle; (**b**) variation in the angular velocity (black curve) and variation in the angular acceleration (red curve).

rotation behavior of the valve cover can be accurately captured, we simulated four drilling fluids and studied their effect on the closing time of the valve cover in section 3.2. Based on section 3.2, among the four simulated drilling fluids, the valve cover exhibited the longest and shortest closing times in the 76% KCOOH and 0.05% XC solution environments, respectively. Therefore, these two representative fluids were employed to study the rotation behavior of the valve cover in different drilling fluid systems. Fig. 7 shows the rotation behavior of the valve cover of the pressure controller in the 76% KCOOH and 0.05% XC solution environments. Fig. 7a and c shows that the variation in the rotation angle in the above two simulated drilling fluids also can be described with the BiDoseResp function. Fig. 7b and d shows the variations in the angular velocity and angular acceleration, respectively, in the 76% KCOOH and 0.05% XC solution environments. As shown in Fig. 7b and d, similar to the results for the water environment described above, elastic and gravitational acceleration zones also existed for these two solutions. However, in the elastic acceleration zone, the initial rotation velocity in the 76% KCOOH and 0.05% XC solutions was 68 and 24°/s lower, respectively, than that in the water environment, and the initial angular acceleration in the two solutions was only 0.086 and 0.233 times that in the water environment. This can be attributed to the stronger adhesion between the back of the valve cover and pipe surface due to the higher solution viscosity. In addition, in contrast to the rotation behavior of the valve cover in the water environment, in the 76% KCOOH and 0.05% XC solution environments, there was no deceleration zone before the gravitational acceleration zone. After the gravitational acceleration zone, the angular velocity of the valve cover in the 76% KCOOH and 0.05% XC solutions started to decrease at 0.34 and 0.24 s, respectively. Overall, the rotation angle in the 76% KCOOH and 0.05% XC solutions can also be described with the BiDoseResp function. An increase in the fluid viscosity increased the adhesion between the back of the valve cover and outer pipe surface, reducing the initial velocity of the valve cover.

4. Discussion

Based on the experimental results, it can be concluded that valve cover rotation in the different environments involves a very complicated process. When the inner pipe was lifted, the elastic piece on the back side of the valve cover provided the initial rotation velocity and rotation acceleration. Thereafter, the valve cover began to rotate around a fixed axis, namely, the pin that is used to connect the valve cover and valve seat. Furthermore, the valve cover can be closed under gravity, and *in-situ* pressure preservation can be achieved. In the air environment, the variation in the rotation angle of the valve cover conformed to the ExpDec1 function, while the angular velocity and angular acceleration of the valve cover increased exponentially over time. In the different fluid environments, the variation in the rotation angle of the valve cover conformed to the BiDoseResp function, while the angular velocity and angular acceleration of the valve cover regularly varied within a certain range. The fluid density and viscosity affected the changes in the angular velocity and angular acceleration and thus impacted the rotation behavior and the final closing time of the valve cover. Notably, the solution density clearly affected the closing time of the valve cover, whereas the effect of viscosity was very slight. In this section, to reveal the mechanisms of the above rotation behavior phenomena of the valve cover in the different environments, we analyzed the rotation process of the valve cover in depth.

4.1. Analysis of the rotation process of the valve cover

A schematic diagram of the rotation process of the valve cover of the pressure controller and the received forces and moments are shown in Fig. 8. As shown in Fig. 8, valve cover rotation is affected by the elastic force of the elastic piece on the back side of the valve cover, gravity, buoyancy and drag resistance of the fluid. The buoyancy satisfies the following:

$$F_B = \rho g V \tag{1}$$

where ρ is the fluid density, g is the gravitational acceleration, and V is the volume of the valve cover.

When the valve cover rotates in a fluid environment, in addition to gravity and buoyancy, the valve cover is affected by the drag resistance of the fluid (Alvarado, 1967):

$$F_R = \frac{1}{2} c \rho s \omega^2 \tag{2}$$

where c is the drag coefficient under steady-state fluid action, ρ is the fluid density, s is the projection area of the valve cover, and ω is the rotation velocity.

The projection area of the valve cover along the direction of rotating motion in a fluid environment is shown in Fig. 9. The

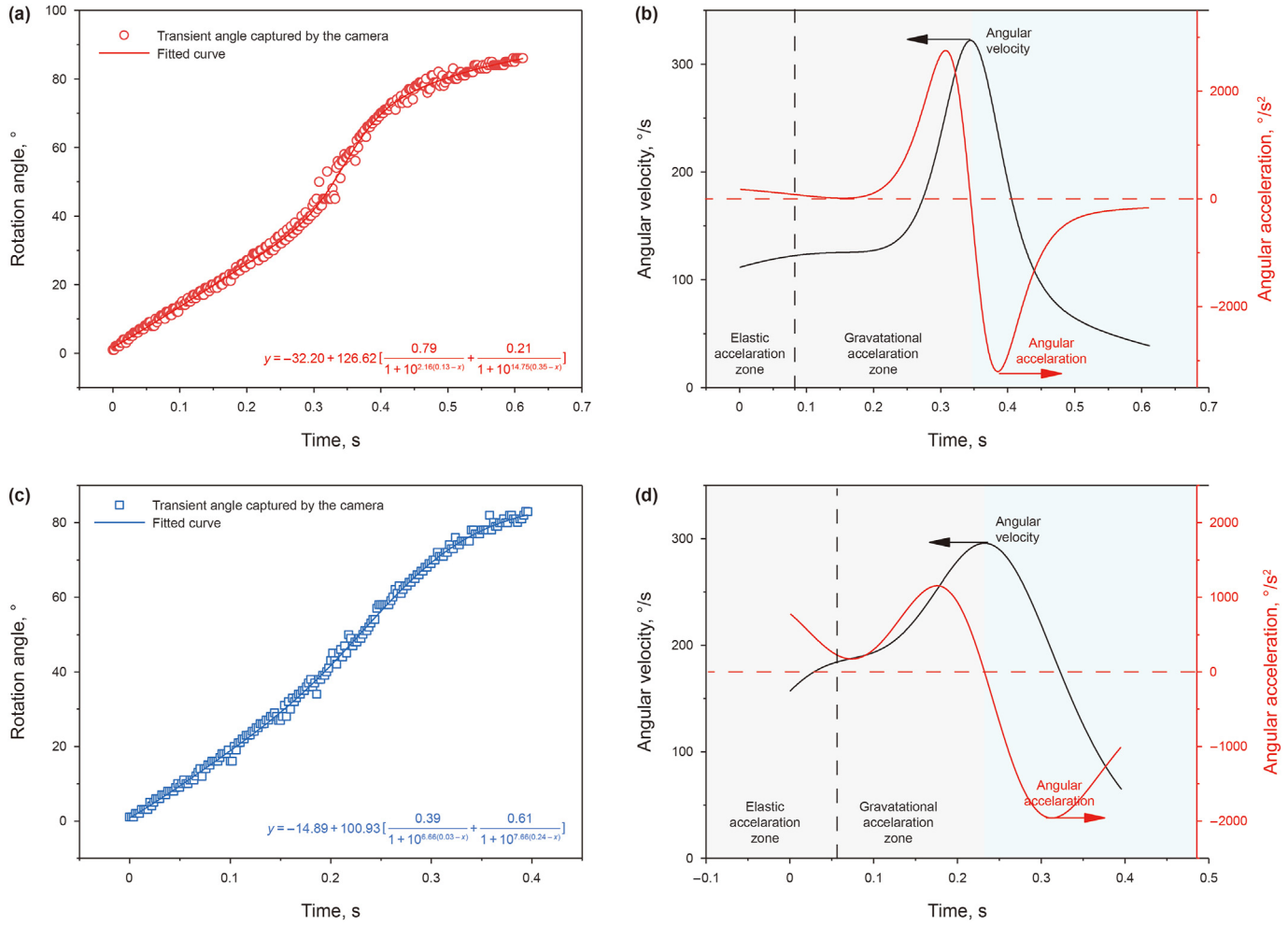

Fig. 7. Rotation behavior of the valve cover of the pressure controller (**a**, **b**) in the 76% KCOOH solution (ρ = 1.565 g/cm^3; AV = 11.85 mPa s) and (**c**, **d**) 0.05% XC solution (ρ = 1.002 g/cm^3; AV = 3.35 mPa s): (**a**, **c**) variation in the rotation angle; (**b**, **d**) variation in the angular velocity (black curves), and variation in the angular acceleration (red curves).

projection area of the valve cover resembles an ellipse, and the length of the long axis of the ellipse is 2a, while the length of the short axis is 2b. A coordinate system can be established with the lower part of the valve cover as the origin, so that the unit area of the projection area of the valve cover meets the following requirements:

$$\mathrm{d}s = 2\sqrt{b^2\left(1-\frac{(r-a)^2}{a^2}\right)}\,\mathrm{d}r \tag{3}$$

where r is the distance from the horizontal axis.

According to Eqs. (2) and (3), the resistance torque due to the drag resistance can be obtained as follows:

$$M_\mathrm{R} = \int_0^{2a}\frac{1}{2}c\rho r\omega^2\mathrm{d}s = \int_0^{2a} c\rho r\omega^2\sqrt{b^2\left(1-\frac{(r-a)^2}{a^2}\right)}\mathrm{d}r \tag{4}$$

Assuming that both gravity and buoyancy act on the center of the valve cover, the rotation torque of the valve cover can be obtained as follows:

$$M = \begin{cases} M_\mathrm{e} + (mg-\rho gV)a\sin\theta - M_\mathrm{R}, (\theta < 10^\circ, \text{elastic action}) \\ (mg-\rho gV)a\sin\theta - M_\mathrm{R}, (\theta > 10^\circ, \text{no elastic action}) \end{cases} \tag{5}$$

where m is the mass of the valve cover, g is the gravitational acceleration, θ is the rotation angle, M_R is the resistance torque due to the drag resistance of the fluid, and M_e is the torque resulting from the elastic force.

The angular acceleration and rotational torque of an object in space are subject to the following relationship (Alvarado, 1967):

$$M = \alpha \cdot I \tag{6}$$

where α is the angular acceleration and I is the moment of inertia, which is an intrinsic parameter of the valve cover and is related to its geometric characteristics and mass.

Therefore, the rotation motion equation of the valve cover can be obtained as follows:

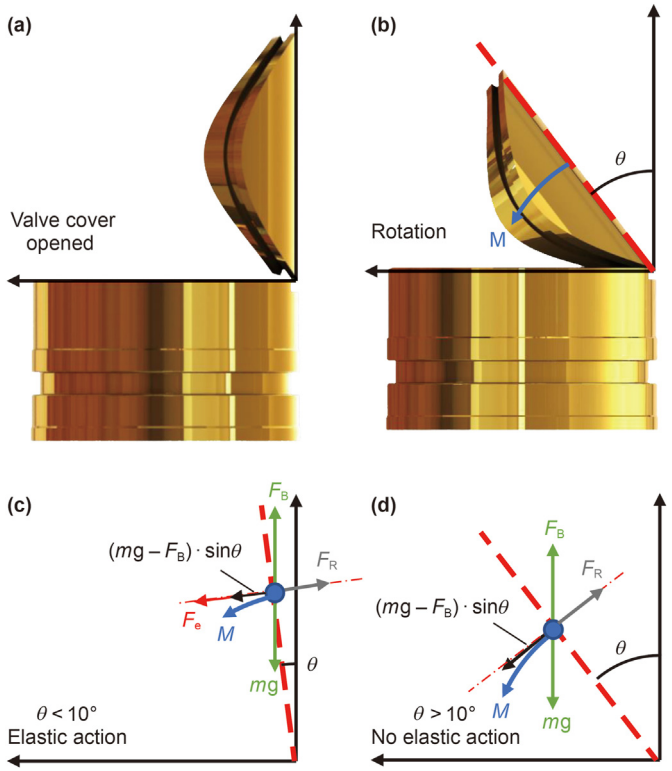

Fig. 8. (**a**, **b**) Schematic diagram of the rotation process of the valve cover of the pressure controller. (**c**, **d**) Force and moment analysis of the valve cover, where m is the mass of the valve cover, g is the gravitational acceleration, θ is the rotation angle, F_B is the buoyancy, F_R is the drag resistance of the fluid, and F_e is the elastic force.

$$\ddot{\theta}\cdot I=\begin{cases} M_e+(mg-\rho gV)a\sin\theta-\left(\int_0^{2a} c\rho r\sqrt{b^2\left(1-\frac{(r-a)^2}{a^2}\right)}\,\mathrm{d}r\right)\cdot\dot{\theta}^2 \\ (\theta<10^\circ,\text{elastic action}) \\ (mg-\rho gV)a\sin\theta-\left(\int_0^{2a} c\rho r\sqrt{b^2\left(1-\frac{(r-a)^2}{a^2}\right)}\,\mathrm{d}r\right)\cdot\dot{\theta}^2 \\ (\theta>10^\circ,\text{no elastic action}) \end{cases} \tag{7}$$

To verify the rotation motion equation of the valve cover established above, we compared the angular acceleration values after the valve cover entered the gravitational acceleration zone ($\theta > 10^\circ$) in the water and 76% KCOOH solution environments obtained by the experiment with the values calculated theoretically using Eq. (7). As shown in Fig. 10, both in the water and in the 76% KCOOH solution environments, the angular acceleration values obtained by theoretical calculation were close to the experimental values, fully reflecting the changes of the angular acceleration of the valve cover. In addition, we performed another experiment in a 66% KCOOH solution environment ($\rho = 1.466$ g/cm^3; AV = 5.25 mPa s) to further verify this functional relation. As shown in Fig. 11a, it was observed that the variation in the rotation angle in the 66% KCOOH solution environment can also be described by a biphasic dose response function, and by taking the second derivative, the experimental result of the angular acceleration in the 66% KCOOH solution can be obtained from the variation in the rotation angle. The comparison of the angular acceleration obtained in the 66% KCOOH solution environment experimentally and by theoretical calculations using

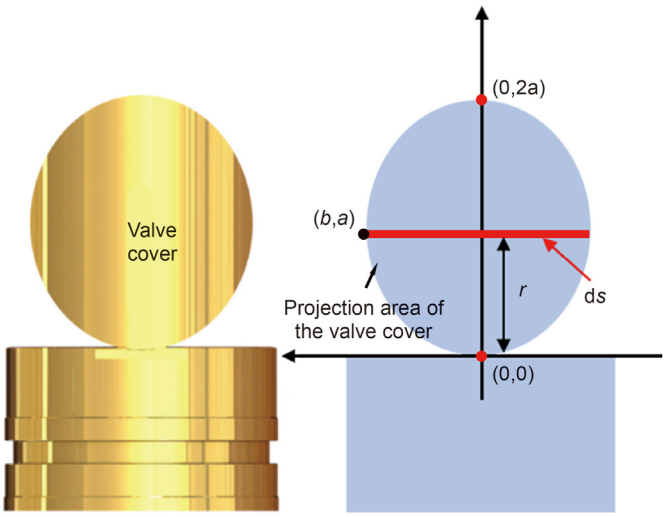

Fig. 9. The projection area of the valve covers along the direction of the rotating motion in a fluid environment.

Eq. (7) was shown in Fig. 11b, it can be observed that the angular acceleration obtained by theoretical calculation using Eq. (7) was still close to the experimental value. Thus, it is proven that the functional relation established above can meet the requirements of this type of valve cover.

For the air environment, the buoyancy and drag resistance almost can be neglected. Thus, Eq. (7) can be simplified as follows:

$$\ddot{\theta}\cdot I=\begin{cases} M_e+mga\sin\theta(\theta<10^\circ,\text{elastic action}) \\ mga\sin\theta(\theta>10^\circ,\text{no elastic action}) \end{cases} \tag{8}$$

Eq. (8) clearly indicates that the angular acceleration ($\ddot{\theta}$ in Eq. (8)) increases with increasing θ, which further results in an exponential increase in the angular velocity and rotation angle over time.

In the various fluid environments, due to the different physical parameters, such as the density and viscosity, the received buoyancy and drag resistance of the valve cover differ. According to Eq. (7), the received buoyancy and drag resistance of the valve cover can directly determine the rotation behavior and final closing time of the valve cover in the different fluids. Following section 3.3.2, in contrast to the rotation behavior of the valve cover in the water environment, in the two simulated drilling fluids, there occurred no deceleration zone before the gravitational acceleration zone. As mentioned in section 3.3, in the water environment, due to the weak adhesion between the valve cover and outer pipe compared with that in the two simulated drilling fluids with high viscosity, the valve cover has a higher initial rotation velocity and initial angular acceleration, as shown in Figs. 6 and 7. The initial velocity in the water environment was 68 and 24°/s higher than those in the 76% KCOOH and 0.05% XC solutions, and the initial angular acceleration in water was 11.6 and 4.3 times than those in the 76% KCOOH and 0.05% XC solutions, respectively. Thus, in the water environment, the valve cover was driven mainly by the elastic force to 10° within only 0.04 s, and the rotation velocity of the valve cover at this time can reach 225°/s; according to Eq. (4), the high rotation velocity will result in a higher resistance torque. Unfortunately, when, $\theta > 10^\circ$, the torque resulting from the elastic force M_e no longer has an effect; rather, at this time, as shown in Eq. (5), due to the resistance torque M_R resulting from the high rotation velocity being too high, above the value of $(mg - \rho gV)a\sin\theta$, the values of the rotation torque M and rotation acceleration drop to negative values, and thus, the valve cover enters a deceleration zone. By

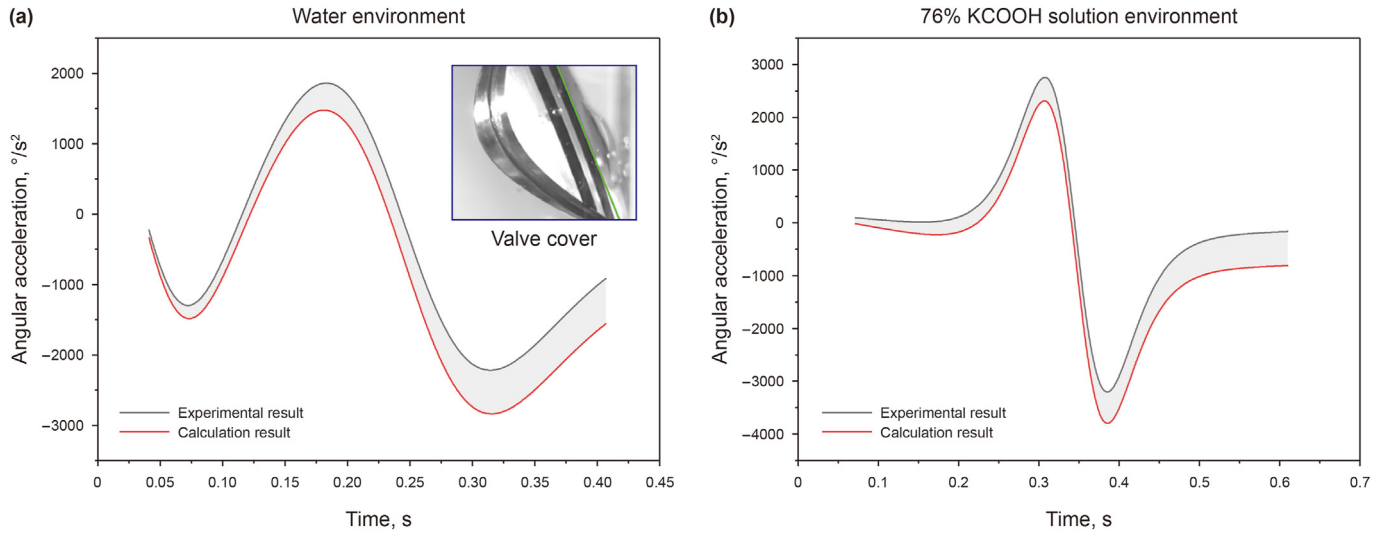

Fig. 10. Comparison of the angular acceleration obtained experimentally and by theoretical calculations using Eq. (7).

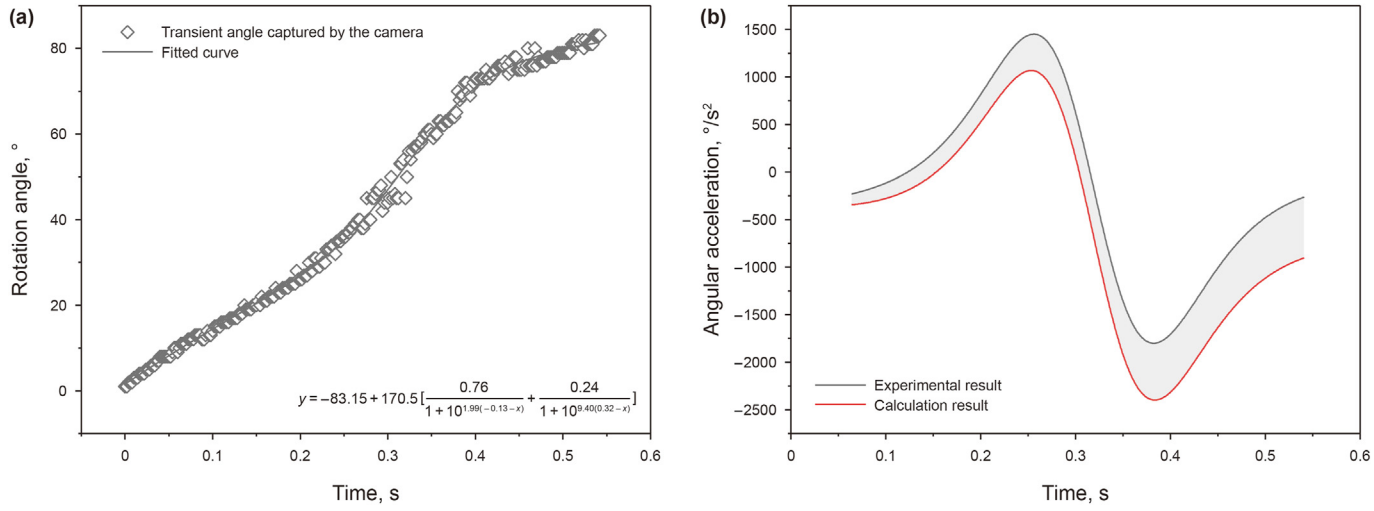

Fig. 11. (**a**) Variation in the rotation angle in a 66% KCOOH solution environment ($\rho = 1.466$ g/cm^3; AV = 5.25 mPa s). (**b**) Comparison of the angular acceleration obtained in a 66% KCOOH solution environment experimentally and by theoretical calculations using Eq. (7).

contrast, as observed from Fig. 7 in the manuscript, in the 76% KCOOH and 0.05% XC solution environments, when the valve cover left the elastic acceleration zone, the instantaneous rotation velocities were only 0.5 and 0.8 times the velocity in the water environment. Thus, according to Eq. (4), the lower rotation velocity will result in a lower resistance torque M_R, and M_R was still lower than the value of $(mg - \rho gV)a \sin\theta$; therefore, there was no deceleration zone before the gravitational acceleration zone. In summary, the instantaneous drag resistance is affected not only by the property of the fluid but also by the instantaneous rotation velocity. In the water environment, due to the higher rotation velocity when the valve cover leaves the elastotic acceleration zone compared with that in the 76% KCOOH and 0.05% XC solutions, the valve cover had higher resistance between the elastic acceleration zone and the gravitational acceleration zone. Thus, a deceleration zone before the gravitational acceleration zone was observed only in the water environment.

On the other hand, it is widely acknowledged that drag resistance consists of viscous resistance and pressure drag components (Sun et al., 2016). Of these, the viscous resistance is attributed to the friction resistance of motion between the fluid layers and is determined by the fluid viscosity, size of the valve cover, and rotation velocity. By contrast, the pressure drag is attributed to fluid boundary layer separation due to inertia during valve cover rotation; this parameter is related to the fluid density, size of the valve cover, and rotation velocity but is unrelated to the viscosity (Sun, 2014). Therefore, it is clear that the fluid density and viscosity affect the pressure drag and viscous resistance components, respectively, of the drag resistance and further impact the rotation behavior and closing time of the valve cover. Notably, according to section 3.2, the solution density clearly affected the closing time of the valve cover, but the viscosity effect was very limited. This suggests that the viscous resistance experienced by the valve cover is very low, but the pressure drag effect is pronounced. Therefore, it can be concluded that the fluid density fluids greatly increase the closing time of the valve cover by increasing the buoyancy and pressure drag. To increase the IPP-Coring success rate in different layers and geological conditions, it is necessary to pay more attention to drilling fluid density changes.

4.2. Drag coefficient variation of the valve cover during the rotation

In various fluid environments, according to Eq. (7), the drag resistance experienced by the valve cover notably impacts its rotation behavior, while the drag coefficient c can remarkably affect the drag resistance, as expressed in Eq. (2). To reveal the mechanisms determining the rotation behavior of the valve cover in various fluid environments, it is necessary to analyze the drag coefficient variation during rotation movement and elucidate the effects of different fluid physical parameters (density and viscosity).

According to the rotation behavior recorded in the experiments, the variation in the drag coefficient can be calculated via Eq. (7). In this study, to simplify the analysis, the variation in the drag coefficient given a rotation angle $\theta > 10^\circ$ was analyzed, i.e., without the effect of elastic action. The solid lines in Fig. 12 show the variation in the drag coefficient, while the dashed lines indicate the variation in the corresponding angular velocity of the valve cover during the experiments. The curves of the drag coefficient of the valve cover in the water and the 0.05% XC solution environments before 0.2 s exhibited slight differences, but the drag coefficients obtained from the whole rotation process of the valve cover were almost identical. Therefore, in this study, it was concluded that the viscosity imposed a negligible effect on the drag coefficient and slightly affected the closing time of the valve cover. In addition, as shown in Fig. 12, the variation in the drag coefficient was negatively correlated with the rotation velocity of the valve cover. For example, in water, when the rotation velocity reached the maximum value of 310°/s in 0.24 s, the drag coefficient reached the minimum value of 0.029. Subsequently, the rotation velocity gradually decreased, but the drag coefficient increased at a continuously-increasing rate. The increase in the drag coefficient was caused not only by the gradually decreasing rotation velocity but also by the increase in the additional boundary damping effect of the outer pipe on the valve cover with increasing rotation angle (Sun, 2014). According to Fig. 12, in the water environment, after the rotation velocity of the valve cover started to drop, the resultant drag coefficient abruptly increased from 0.045 to 1.3 within 0.16 s. However, in the 76% KCOOH solution with a higher density, the drag coefficient experienced by the valve cover increased to a value of 1.43 from 0.016 within a longer period of 0.26 s. This indicates that in the 76% KCOOH solution, the valve cover experienced relatively higher drag coefficients during longer periods than those in the other solutions, further increasing the closing time of the valve cover. Generally, the variation in the drag coefficient was negatively correlated with the rotation velocity. In addition, the fluid viscosity exerted a negligible effect on the drag coefficient, while the density altered the period during which the valve cover experienced a higher drag coefficient and further impacted the rotation behavior.

4.3. Control schemes for the rotation behavior of the valve cover during IPP-Coring in different layers and geological conditions

In the practice of IPP-Coring, the air environment is only applicable in a few unique cases, and in these cases the rotation behavior of the valve cover is relatively simple. In most cases, the valve cover can be suitably adopted in fluid environments. Based on the experimental results and discussion above, in fluid environments, the rotation behavior is affected by the fluid density and viscosity. The main effects and corresponding effect mechanisms of the viscosity and density of drilling fluids on the rotation behavior of the valve cover are summarized in Fig. 13. Although the effect of the viscosity on the rotation behavior and total closing time is limited, it increases the adhesion between the valve cover and outer pipe and further decreases the initial rotation velocity and acceleration. However, an increase in the fluid density increases the buoyancy and the period during which the valve cover is subjected to a higher drag coefficient. Therefore, the fluid density can further affect the rotation behavior of the valve cover and increase the total closing time. Thus, control schemes for the rotation behavior of the valve cover during IPP-Coring in different layers and geological conditions can be determined. During IPP-Coring in layers requiring the use of high-viscosity drilling fluids, such as the leakage layer, control of the adhesion between the valve cover and outer pipe is the key for controlling the rotation behavior and closing time of the valve cover. As shown in Fig. 13, to reduce adhesion, the contact area between the valve cover and outer pipe

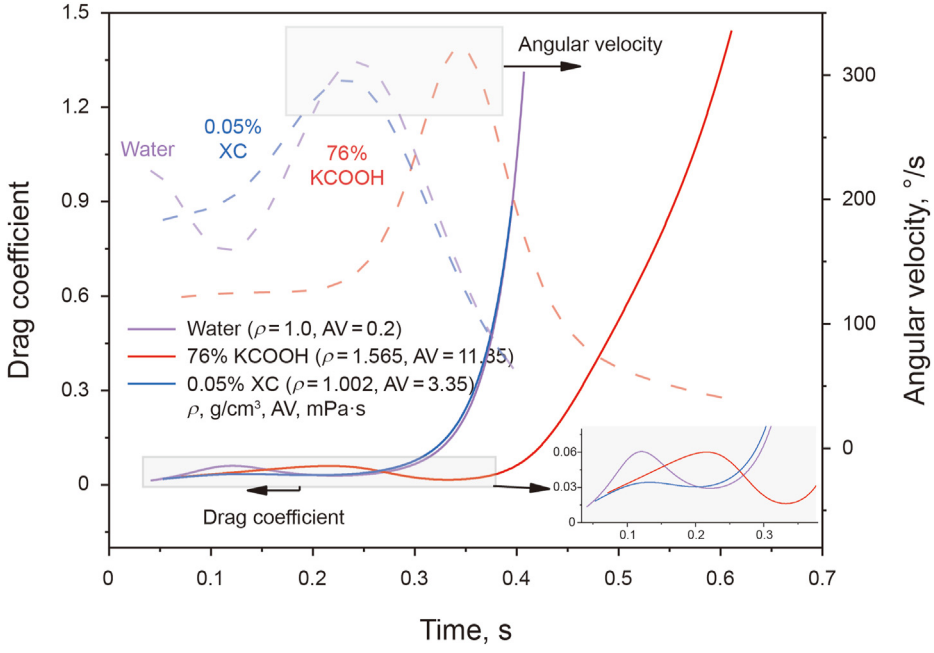

Fig. 12. Variation in the drag coefficient (solid lines) and variation in the corresponding angular velocity of the valve cover (dashed lines).

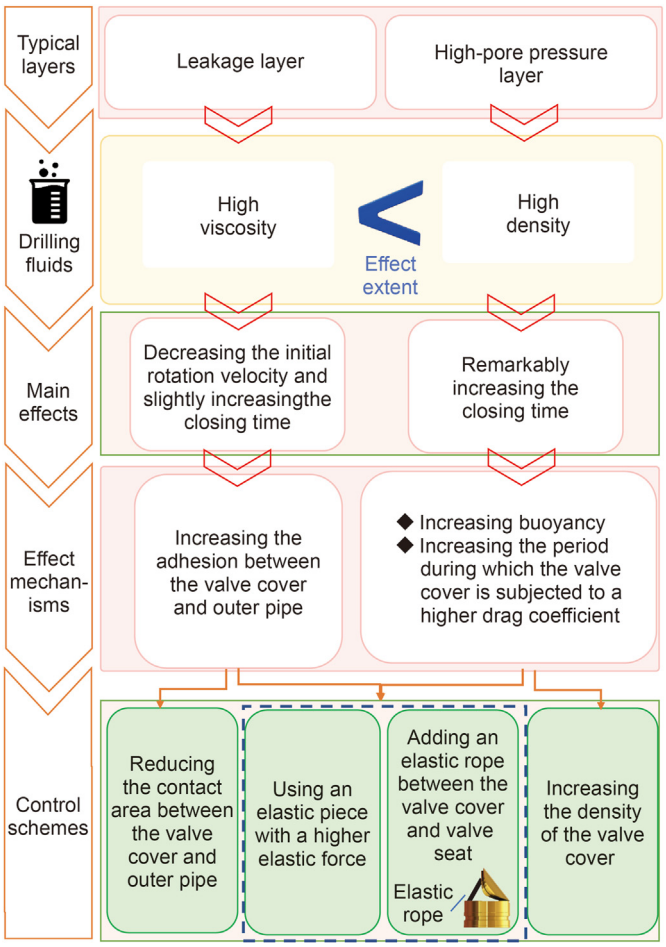

Fig. 13. Summary of the main effects and effect mechanisms of the fluid viscosity and density on the rotation behavior of the valve cover and control schemes for the rotation behavior of the valve cover during IPP-Coring in different layers and geological conditions.

can be reduced. During coring in the layers involving the use of high-density drilling fluids, such as the high-pore pressure layer, controlling the density difference between the valve cover and drilling fluid is the key to controlling the rotation behavior and closing time of the valve cover. As shown in Fig. 13, the use of a high-density metal as the material of the valve reduces the final closing time. In addition, including a new action field, such as elastic and magnetic fields (Liu et al., 2020), can effectively control the rotation behavior and closing time of the valve cover. As shown in Fig. 13, in the layers requiring the use of either high-viscosity or high-density drilling fluids, ether the use of an elastic piece with a higher elastic force or addition of an elastic rope between the valve cover and valve seat, respectively, can increase both the rotation velocity and total closing time of the valve cover.

5. Conclusions

In this study, the closing time and rotation behavior of the valve cover in different environments were obtained using a high-speed camera. The mechanisms of the rotation behavior of the valve cover in the different environments were elucidated by a thorough analysis of the rotation process and variation in the drag coefficient of the valve cover. Based on the results, control schemes for the rotation behavior of the valve cover during IPP-Coring in different layers and geological conditions were proposed. The specific conclusions can be summarized as follows.

1. The fluid density clearly affected the closing time of the valve cover, but the effect of the viscosity was quite limited. In the 76% KCOOH solution, with a density 1.565 times that of water, the valve cover attained the longest closing time of 0.626 s, which is 3.82 and 1.53 times higher than those in air and water, respectively. The closing time of the valve cover in the 0.05% and 0.15% XC solutions with apparent viscosities 16.6 and 41.75 times higher than that of water, respectively, approached the closing time in water.
2. The variation in the rotation angle of the valve cover in the air and fluid environments can be described with the ExpDec1 and BiDoseResp functions, respectively. In the air environment, the angular velocity and angular acceleration of the valve cover increased exponentially over time. However, in the various fluid environments, the rotation behavior revealed distinct elastic and gravitational acceleration zones, while the angular velocity and angular acceleration of the valve cover regularly varied within a certain range.
3. The variation in the drag coefficient was negatively correlated with the rotation velocity. In addition, the viscosity imposed a negligible effect on the drag coefficient, but increased the adhesion between the valve cover and outer pipe and further decreased the initial rotation velocity and acceleration. The density increased the buoyancy and the period during which the valve cover was subjected to a higher drag coefficient, further altering the rotation behavior and increasing the closing time.
4. In the layers requiring the use of high-viscosity drilling fluids, such as the leakage layer, the key to controlling the rotation behavior of the valve cover is to control the adhesion between the valve cover and outer pipe of the IPP-Coring devices. During coring in layers involving the application of high-density drilling fluids, such as the layers with high pore pressure, controlling the density difference between the valve cover and drilling fluid is the key to controlling the rotation behavior. In addition, inclusion of a new action field, such as an elastic or magnetic field, can effectively control the rotation behavior and closing time of the valve cover.

Declaration of competing interest

The authors declare that they have no known competing financial interests or personal relationships that could have appeared to influence the work reported in this paper.

Acknowledgments

The authors are grateful for the financial support from the National Natural Science Foundation of China (No. 51827901 & No. 52274133) and the Program for Guangdong Introducing Innovative and Enterpreneurial Teams (No. 2019ZT08G315) and the Shenzhen National Science Fund for Distinguished Young Scholars (RCJC20210706091948015).

References

Abid, K., Spagnoli, G., Teodoriu, C., et al., 2015. Review of pressure coring systems for offshore gas hydrates research. Underw. Technol. 33 (1), 19–30. https://doi.org/10.3723/ut.33.019.

Ali, M., Hegazy, G.M., Aftab, M.N., et al., 2014. First wireline and elevated pressure coring in UAE - saved 30% of coring time for shallow reservoirs & delivered realistic fluids and gas saturations. In: Abu Dhabi International Petroleum Exhibition & Conference, 10–13 November, Abu Dhabi, UAE. https://doi.org/10.2118/171866-MS.

Al Saman Al Neaimi, M., Tee, A.S.C., Boyd, D., et al., 2014. Acquisition of an elevated pressure core in a gas flooded carbonate oil reservoir: design and operational

challenges. In: Abu Dhabi International Petroleum Exhibition and Conference, 10–13 November, Abu Dhabi, UAE. https://doi.org/10.2118/171815-MS.
Alvarado, U., 1967. A method for obtaining high fidelity underwater simulation of mannedspace activities. In: 4th Annual Meeting and Technical Display. 23–27 October, Anaheim, CA, U.S.A. https://doi.org/10.2514/6.1967-925.
Ashena, R., 2017. Optimization of Core Tripping Using a Thermoporoelastic Approach. Montanuniversität Leoben.
Ashena, R., Thonhauser, G., 2018. Coring Methods and Systems. https://doi.org/10.1007/978-3-319-77733-7.
Aydin, G., 2015. Regression models for forecasting global oil production. Petrol. Sci. Technol. 33 (21–22), 1822–1828. https://doi.org/10.1080/10916466.2015.1101474.
Bjorum, M., 2013. A new coring technology to quantify hydrocarbon content and saturation. In: SPE Unconventional Resources Conference Canada, 5–7 November, Calgary, Alberta, Canada. https://doi.org/10.2118/167228-MS.
Burger, J., Gupta, D., Jacobs, P., et al., 2003. Overview on Hydrate Coring, Handling and Analysis. Technical Report, United States. https://doi.org/10.2172/908303.
Davis, M., Williams, R., Willberg, D., et al., 2013. Novel controlled pressure coring and laboratory methodologies enable quantitative determination of resource-in-place and PVT behavior of the Duvernay shale. In: SPE Unconventional Resources Conference Canada, 5–7 November, Calgary, Alberta, Canada. https://doi.org/10.2118/167199-MS.
Dickens, G.R., Paull, C.K., Wallace, P., 1997. Direct measurement of in situ methane quantities in a large gas-hydrate reservoir. Nature 385 (6615), 426–428. https://doi.org/10.1038/385426a0.
Dickens, G.R., Schroeder, D., Hinrichs, K., 2003. The pressure core sampler (PCS) on ODP leg 201: general operations and gas release. In: Proc. Ocean Drill. Program. https://doi.org/10.2973/ODP.PROC.IR.201.103.2003, 201 Initial Reports.
Gao, M.Z., Chen, L., Fan, D., et al., 2021. Principle and technology of coring with in-situ pressure and gas maintaining in deep coal mine. J. China Coal Soc. 46 (3), 885–897. https://doi.org/10.13225/j.cnki.jccs.YT21.0297 (in Chinese).
Gautam, S., Guria, C., Rajak, V., 2022. A state of the art review on the performance of high-pressure and high-temperature drilling fluids: towards understanding the structure-property relationship of drilling fluid additives. J. Pet. Sci. Eng. 213, 110318. https://doi.org/10.1016/j.petrol.2022.110318.
He, Z.Q., Chen, L., Lu, T., et al., 2019. The optimization of pressure controller for deep earth drilling. Therm. Sci. 23 (Suppl. 3), 877–885. https://doi.org/10.2298/TSCI180612123H.
He, Z.Q., Yang, Y., Yu, B., et al., 2022. Research on properties of hollow glass microspheres/epoxy resin composites applied in deep rock in-situ temperature-preserved coring. Petrol. Sci. 19 (2), 720–730. https://doi.org/10.1016/j.petsci.2021.10.028.
Hu, Y.Q., Xie, J., Xue, S.N., et al., 2022. Research and application of thermal insulation effect of natural gas hydrate freezing corer based on the wireline-coring principle. Petrol. Sci. 19 (3), 1291–1304. https://doi.org/10.1016/j.petsci.2021.11.019.
Huang, W., Feng, G., He, H.L., et al., 2021. Development of an ultra-high-pressure rotary combined dynamic seal and experimental study on its sealing performance in deep energy mining conditions. Petrol. Sci. 19 (3), 1305–1321. https://doi.org/10.1016/j.petsci.2021.11.020.
Hyland, C.R., 1983. Pressure coring-an oilfield tool. In: SPE Annual Technical Conference and Exhibition, 5–8 October, San Francisco, California. https://doi.org/10.2118/12093-MS.
Kawasaki, M., Umezu, S., Yasuda, M., 2006. Pressure temperature core sampler(PTCS). J. Japanese Assoc. Pet. Technol. 71 (1), 139–147. https://doi.org/10.3720/japt.71.139.
Kvenvolden, K.A., Barnard, L.A., Cameron, D.H., 1983. Pressure core barrel: application to the study of gas hydrates. Deep Sea Drilling Project Site 533. https://doi.org/10.2973/dsdp.proc.76.107.1983. Leg 76. Initial reports DSDP, Leg 76.
Li, C., Pei, J.L., Wu, N.H., et al., 2022a. Rotational failure analysis of spherical-cylindrical shell pressure controllers related to gas hydrate drilling investigations. Petrol. Sci. 19 (2), 789–799. https://doi.org/10.1016/j.petsci.2022.02.005.
Li, C., Xie, H.P., Gao, M.Z., et al., 2021. Novel designs of pressure controllers to enhance the upper pressure limit for gas-hydrate-bearing sediment sampling. Energy 227, 120405. https://doi.org/10.1016/j.energy.2021.120405.
Li, J.N., Wang, J., Hu, Y.Q., et al., 2022b. Contact performance analysis of pressure controller's sealing interface in deep *in-situ* pressure-preserved coring system. Petrol. Sci. 19 (3), 1334–1346. https://doi.org/10.1016/j.petsci.2021.11.022.
Liu, G.K., Gao, M.Z., Yang, Z.W., et al., 2020. The innovative design of deep in situ pressure retained coring based on magnetic field trigger controller. Adv. Civ. Eng. 2020, 8873628. https://doi.org/10.1155/2020/8873628.
Mahmoud, H., Hamza, A., Nasser, M.S., et al., 2020. Hole cleaning and drilling fluid sweeps in horizontal and deviated wells: comprehensive review. J. Pet. Sci. Eng. 186, 106748. https://doi.org/10.1016/j.petrol.2019.106748.
Mahzari, P., Mitchell, T.M., Jones, A.P., et al., 2021. Direct gas-in-place measurements prove much higher production potential than expected for shale formations. Sci. Rep. 11, 10775. https://doi.org/10.1038/s41598-021-90160-3.
Mukherjee, P., Peres, J., Hayat, L., et al., 2018. First-ever large diameter fully captured & retained pressurized core and in-situ analysis with slow depressurization - pilot case on giant burgan reservoir. In: Abu Dhabi International Petroleum Exhibition & Conference, 12–15 November, Abu Dhabi, UAE. https://doi.org/10.2118/193021-MS.
Qin, H.W., Gu, L.Y., Li, S.L., et al., 2005. Pressure tight piston corer - a new approach on gas hydrate investigation. China Ocean Eng. 019 (001), 121–128.
Sahu, C., Kumar, R., Sangwai, J.S., 2020. Comprehensive review on exploration and drilling techniques for natural gas hydrate reservoirs. Energy Fuel. 34 (10), 11813–11839. https://doi.org/10.1021/acs.energyfuels.0c02202.
Sun, B., Guo, Y., Wang, Z., et al., 2015a. Experimental study on the drag coefficient of single bubbles rising in static non-Newtonian fluids in wellbore. J. Nat. Gas Sci. Eng. 26, 867–872. https://doi.org/10.1016/j.jngse.2015.07.020.
Sun, X.F., 2014. Experimental Study on Hole Cleaning and Cleaning Tool Optimal Design in Highly- Deviated Hole. Northeast Petroleum University (in Chinese).
Sun, X.F., Ji, G.D., Feng, S.L., et al., 2016. Cuttings particle settling velocity within power law fluid. Fault-Block Oil Gas Field 23 (1), 120–124 (in Chinese).
Sun, Y., Wang, Y., Lü, X., et al., 2015b. Hole-bottom freezing method for gas hydrate sampling. J. Nat. Gas Sci. Eng. 25, 271–283. https://doi.org/10.1016/j.jngse.2015.05.011.
Wang, H., Ge, Y., Shi, L., et al., 2017. Technologies in deep and ultra-deep well drilling: present status, challenges and future trend in the 13th Five-Year Plan period (2016–2020). Nat. Gas. Ind. B. 4 (5), 319–326. https://doi.org/10.1016/j.ngib.2017.09.001.
Xie, H.P., Gao, F., Ju, Y., 2015. Research and development of rock mechanics in deep grounp engineering. Chin. J. Rock Mech. Eng. 34, 2161–2678. https://doi.org/10.13722/j.cnki.jrme.2015.1369 (in Chinese).
Xie, H.P., Gao, M.Z., Zhang, R., et al., 2020. Study on concept and progress of in situ fidelity coring of deep rocks. Chin. J. Rock Mech. Eng. 39 (5), 865–876 doi: 10.13722/j.cnki.jrme.2020.0138 (in Chinese).
Xie, H.P., Liu, T., Gao, M.Z., et al., 2021. Research on in-situ condition preserved coring and testing systems. Petrol. Sci. 18 (6), 1840–1859. https://doi.org/10.1016/j.petsci.2021.11.003.
Yang, L.W., Sun, W.T., Luo, J., et al., 2014. Study and application of GWY194-70BB heat and pressure preservation coring tool. OIL Drill. Prod. Technol. 36 (5), 58–61 (in Chinese).
Yang, L.W., Su, Y., Luo, J., et al., 2020. Development and application of GW-CP194-80A pressure-maintaining coring tool. Nat. Gas. Ind. 40 (4), 91–96 (in Chinese).
You, Z.X., Chen, L., Li, C., et al., 2022. Cutting migration and core disturbance caused by the hydraulic structure of pressure- and gas-maintaining coring bits. Geofluids. https://doi.org/10.1155/2022/9728046, 2022.
Zhang, K.B., 2019. The Prediction Model of Cutting Particles Settling and its Reciprocation Angle. Northeast Petroleum University (in Chinese).
Zhu, H.Y., Liu, Q.Y., Deng, J.G., et al., 2011. Pressure and temperature preservation techniques for gas-hydrate-bearing sediments sampling. Energy 36 (7), 4542–4551. https://doi.org/10.1016/j.energy.2011.03.053.
Zhu, H.Y., Liu, Q.Y., Wong, G.R., et al., 2013. A pressure and temperature preservation system for gas-hydrate-bearing sediments sampler. Petrol. Sci. Technol. 31 (6), 652–662. https://doi.org/10.1080/10916466.2010.531352.